

Transverse and forward energy distributions in ultrarelativistic heavy-ion collisions by an absorption model

K. C. Chung, C. S. Wang,* A. J. Santiago, and G. Pech

Departamento de Física Nuclear e Altas Energias, Instituto de Física, Universidade do Estado do Rio de Janeiro, Rio de Janeiro-RJ, 20559-900, Brazil

(Received 30 July 1997)

An absorption model based on the eikonal approximation of the nuclear optical model is proposed for the transverse and the forward energy distributions in ultrarelativistic heavy-ion collisions. It is shown that the measured distributions can be expressed by their geometric distribution convoluted by a Gaussian distribution with centroid and width determined by the collision geometry and the average properties of N - N collisions. This result provides a physical argument for the formula used in the data fitting of the transverse energy distribution in the literature. The forward energy distribution formula is shown to be applicable for the data fitting. [S0556-2813(98)05902-0]

PACS number(s): 25.75.-q

I. INTRODUCTION

Ultrarelativistic heavy-ion collisions have become the focus of intense research because of the possibility of producing a deconfined quark-gluon plasma as well as of restoring chiral symmetry during such collisions [1]. The global observables, i.e., the transverse energy, the forward energy, the multiplicity, the rapidity, and the transverse momentum distributions of the created particles—mainly pions and other hadrons in addition to photons and leptons—are understood as the observables related mainly to the collision geometry and kinematics, and thus are important for understanding the collision mechanism itself.

Actually, the transverse energy, the forward energy, and the multiplicity distributions have been used to control the centrality of collisions in high energy nucleus collision experiments. Especially, in the recent measured anomalous J/ψ suppression in Pb+Pb collisions at 158A GeV/c [2] which has attracted much attention [3], the transverse energy has been used as centrality cuts since each transverse energy range is shown to correspond to an average impact parameter.

However, the correlation between the collision centrality and the global observables, for example, the transverse energy distribution, is model dependent. Even some specific models for the global observables exist already [4–16]; in addition to several microscopic model calculations such as by FRITIOF, RQMD, VENUS or HIJING, a phenomenological model of global observables, which is reliable in theoretical formulation and easy in numerical application, is still needed in interpreting the centrality dependence of the measured data [17,18].

As the global observables are related mainly to the collision geometry and kinematics which are not sensitive to the microscopic degrees of freedom of the colliding system, the relativistic nuclear optical model is an appropriate scheme for formulating such a kind of phenomenological model. In

the optical model, the interaction between the projectile and the target is expressed by a potential with an imaginary part, and this potential describes the collision geometry in an intuitive and very simple way [19]. On the other hand, it is well known that the nuclear optical model in high energy nuclear collision processes is just the limit of the Glauber multiple collision theory [20–22] for a large number of nucleons; thus it can be interpreted on the basis of the multiple collision picture.

The purpose of this paper is to develop a phenomenological model, based on the eikonal approximation of the relativistic nuclear optical model, for the transverse and the forward energy distributions in ultrarelativistic heavy-ion collisions, and to use it to discuss the physics as well as the geometry involved in the collisions. Section II outlines the eikonal approximation approach of the nuclear optical model for high energy collisions, Sec. III treats the transverse energy distribution, Sec. IV formulates the forward energy distribution, Sec. V gives some numerical examples in applying these formulas, and Sec. VI is a short discussion and summary.

II. EIKONAL APPROXIMATION APPROACH OF THE NUCLEAR OPTICAL MODEL

Following the nuclear optical model [19], a phenomenological potential involving a real part and an imaginary part can be assumed for the collision between projectile particle p and target A , $p+A$,

$$V(\mathbf{r}) = V_0(\mathbf{r}) - iW(\mathbf{r}). \quad (1)$$

The real part $V_0(\mathbf{r})$ describes the elastic scattering, and the imaginary part $W(\mathbf{r})$ describes the absorption of the incoming wave by the target. The absorption of the incoming wave means a decrease of the outgoing wave. This is equivalent to the inelastic process, including the actual absorption of the projectile and the creation of new particles, beside the inelastic scattering of the projectile.

For high energy processes, the Dirac equation should be used for the wave function Ψ of the projectile of mass m ,

*Permanent address: Department of Technical Physics, Peking University, Beijing 100871, China.

$$i\hbar \frac{\partial \Psi}{\partial t} = [-i\hbar c \boldsymbol{\alpha} \cdot \nabla + \beta mc^2 + V(\mathbf{r})] \Psi, \quad (2)$$

where $\boldsymbol{\alpha}$ and β are the Dirac 4×4 matrices. The corresponding continuity equation is

$$\nabla \cdot \mathbf{j} + \frac{\partial \rho}{\partial t} = \frac{2}{\hbar} \text{Im} V(\mathbf{r}) \rho, \quad (3)$$

where $\rho = \Psi^\dagger \Psi$ and $\mathbf{j} = c \Psi^\dagger \boldsymbol{\alpha} \Psi$ are the probability density and the probability current density, respectively. Since the right-hand side of the continuity equation is the source of the current, the imaginary part of the potential is proportional to the strength of absorption—or equivalently the strength of the inelastic process.

For the stationary state with energy E , $\Psi = e^{-iEt/\hbar} \psi(\mathbf{r})$, the incoming wave with momentum $p_0 = \hbar k_0$ along the z axis is

$$\psi_{\text{in}}(\mathbf{r}) = e^{ik_0 z} u(p_0), \quad (4)$$

where $u(p_0)$ is the Dirac spinor. In the eikonal approximation, the wave function corresponding to the above incoming wave is

$$\psi_{\text{eikonal}}(\mathbf{r}) = e^{ik_0 z + i\gamma(\mathbf{r})} u(p_0), \quad (5)$$

where the eikonal phase shift $\gamma(\mathbf{r})$ is

$$\gamma(\mathbf{r}) \approx -\frac{E}{\hbar^2 c^2 k_0} \int_{-\infty}^z V(\mathbf{r}) dz. \quad (6)$$

The conditions under which this eikonal approach holds are $E \gg |V(\mathbf{r})|$ and $mc^2, k_0 \gg |\nabla \gamma(\mathbf{r})|$, and $\mathbf{p}_0 \times \nabla \gamma(\mathbf{r}) \approx 0$.

In this eikonal approximation, the outgoing wave for $r \rightarrow \infty$ can be shown as

$$\Psi_{\text{out}}(\mathbf{r}) = \frac{e^{ikr}}{r} f(\theta, \phi) u_{\text{out}}(p, p_0), \quad (7)$$

where

$$u_{\text{out}}(p, p_0) = \frac{1}{2E} (E + \beta mc^2 + c \boldsymbol{\alpha} \cdot \mathbf{p}) u(p_0) \quad (8)$$

and

$$\begin{aligned} f(\theta, \phi) &= -\frac{1}{4\pi} \frac{2E}{\hbar^2 c^2} \int d^3 \mathbf{r} e^{i\mathbf{q} \cdot \mathbf{r} + i\gamma(\mathbf{r})} V(\mathbf{r}) \\ &= \frac{k_0}{2\pi i} \int d^2 \mathbf{b} e^{i\mathbf{q} \cdot \mathbf{b}} [e^{i\chi(\mathbf{b})} - 1]. \end{aligned} \quad (9)$$

In the above equation, $\hbar \mathbf{q} = \hbar(\mathbf{k}_0 - \mathbf{k})$ is the momentum transfer with $k_0 = k$, θ is the angle between \mathbf{k} and \mathbf{k}_0 , and

$$\chi(\mathbf{b}) = \gamma(\mathbf{b}, z \rightarrow \infty) = -\frac{E}{\hbar^2 c^2 k_0} \int_{-\infty}^{\infty} V(\mathbf{b}, z) dz, \quad (10)$$

where \mathbf{b} is the plane vector perpendicular to $(\mathbf{k}_0 + \mathbf{k})$. In high energy processes, where θ is very small, \mathbf{b} is approximately

the impact parameter. It should be noted that Eq. (9) is exactly the same as that obtained by the relativistic Feynman diagram technique [23,24].

Following the standard procedure for deriving the optical theorem in the nonrelativistic potential scattering theory [19], the generalized optical theorem can be derived from the continuity equation based on the relativistic outgoing wave function (7), giving as a result $\sigma = \sigma^s + \sigma^a$, where σ is the total cross section, σ^s the total elastic scattering cross section, and σ^a the total absorption cross section, respectively,

$$\sigma = \frac{4\pi}{k_0} \text{Im} f(\theta=0) = 2 \text{Re} \int d^2 \mathbf{b} [1 - e^{i\chi(\mathbf{b})}], \quad (11)$$

$$\begin{aligned} \sigma^s &= \int d\Omega |f(\theta, \phi)|^2 u_{\text{out}}^\dagger(p, p_0) u_{\text{out}}(p, p_0) \\ &= \int d^2 \mathbf{b} |e^{i\chi(\mathbf{b})} - 1|^2, \end{aligned} \quad (12)$$

$$\begin{aligned} \sigma^a &= -\frac{E}{\hbar^2 c^2 k_0} \int d^3 \mathbf{r} 2 \text{Im} V(\mathbf{r}) e^{-2\text{Im}\gamma(\mathbf{r})} \\ &= \int d^2 \mathbf{b} [1 - e^{-2\text{Im}\chi(\mathbf{b})}]. \end{aligned} \quad (13)$$

The above formulas give the relationships between the measurable quantities σ , σ^s , and σ^a and the dynamical quantities $V_0(\mathbf{r})$ and $W(\mathbf{r})$ through the eikonal phase shift at infinity $\chi(\mathbf{b})$. As we are concerned with the inelastic process only, the relevant dynamical quantity in the present work is the imaginary part of the potential $W(\mathbf{r})$. It is interesting to note that the right-hand side of the above formulas is exactly the same as that of the corresponding nonrelativistic ones; the only difference is given by the factor in front of the integral in Eq. (10).

In the nuclear optical model, two terms are assumed phenomenologically for $W(\mathbf{r})$ [25]. The first term is proportional to the target nucleus density $\rho_A(\mathbf{r})$ and is used to describe the volume effect of the collision. The second term is proportional to both the radial derivative of the nuclear density and the range of the force between the colliding particles, and is used to describe the surface effect of the collision. In high energy processes, it is believed that the surface effect of the collision can be neglected in a rough approximation, in the present stage of our study, and we can assume

$$W(\mathbf{r}) = w \rho_A(\mathbf{r}), \quad (14)$$

where w is a model parameter representing the interaction strength between the colliding particles. By this assumption, we have

$$2\text{Im}\chi(\mathbf{b}) = \frac{2E}{\hbar^2 c^2 k_0} \int_{-\infty}^{\infty} W(\mathbf{b}, z) dz = \sigma_0 D_A(\mathbf{b}), \quad (15)$$

where

$$\sigma_0 = \frac{2Ew}{\hbar^2 c^2 k_0} \quad (16)$$

and

$$D_A(\mathbf{b}) = \int_{-\infty}^{\infty} \rho_A(\mathbf{b}, z) dz \quad (17)$$

is the thickness distribution function of the target.

Using this result, the total absorption cross section is

$$\sigma^a = \int d^2\mathbf{b} [1 - e^{-\sigma_0 D_A(\mathbf{b})}] = \int d^2\mathbf{b} [1 - S_{pA}(\mathbf{b})], \quad (18)$$

where

$$S_{pA}(\mathbf{b}) = e^{-\sigma_0 D_A(\mathbf{b})} \quad (19)$$

is the transmission coefficient of target A against the projectile p . The quantity $\sigma_0 D_A(\mathbf{b}) = -\ln S_{pA}(\mathbf{b})$ can be interpreted as the opaqueness of the target against the projectile at the impact parameter \mathbf{b} [26]. For very large opaqueness, $\sigma_0 D_A(\mathbf{b}) \gg 1$ for $0 \leq b \leq b_{\max}$ where b_{\max} is the maximum impact parameter beyond which the target thickness is zero, i.e. $D_A(b \geq b_{\max}) = 0$, the total absorption cross section equals the geometric cross section, $\sigma^a = \pi b_{\max}^2$, and the target looks like a black disk. In this consideration, the simple sharp radius model of nuclei has been used. On the other hand, for very small opaqueness, $\sigma_0 D_A(\mathbf{b}) \ll 1$, the total absorption cross section equals σ_0 times A ,

$$A = \int d^3\mathbf{r} \rho_A(\mathbf{r}), \quad (20)$$

and the target looks transparent. Generally, the total absorption cross section is larger than $\sigma_0 A$ but less than the geometric cross section, $\sigma_0 A \leq \sigma^a \leq \pi b_{\max}^2$; i.e., the target looks like a gray disk. As the transmission coefficient $S_{pA}(\mathbf{b}) = \exp[-\sigma_0 D_A(\mathbf{b})]$ shows an exponential decrease of the current along the path in the target with thickness distribution $D_A(\mathbf{b})$, σ_0 can be interpreted as the effective cross section of the projectile when it passes through the target. It should be emphasized here that σ_0 is the free particle-particle inelastic cross section only in the transparent case when we have $\sigma^a = \sigma_0 A$. Generally, σ_0 depends on the nuclear density and should be regarded as an adjustable parameter determined by the measured data.

The total absorption cross section (18) can be rewritten as

$$\sigma^a = \sum_{n=1}^{\infty} \frac{1}{n!} \int d^2\mathbf{b} e^{-\sigma_0 D_A(\mathbf{b})} [\sigma_0 D_A(\mathbf{b})]^n. \quad (21)$$

It can be seen that the above formula resembles that obtained by applying the Glauber theory to high energy nuclear multiple collision processes. Since the optical model is the limit of the Glauber multiple collision theory for a large number of nucleons, the above formula allows us to understand the absorption process in this case as a Glauber multiple collision where n is the number of elemental collisions. The difference is that in the Glauber theory the nucleon is considered as the elemental constituent of the target, while in the optical model a droplet of some finely granulated scattering medium, which is composed of an infinite number of particles with infinitesimal size, is assumed for the target [26].

III. TRANSVERSE ENERGY DISTRIBUTION

In order to work out the formulas for the transverse and the forward energy distributions, further consideration and assumptions are required. As the parameter σ_0 can be understood as the effective collision cross section between the projectile and the target particle, it can be written as an integral over the transverse energy distribution of this collision,

$$\sigma_0 = \int d\varepsilon_T \frac{d\sigma_0}{d\varepsilon_T}. \quad (22)$$

Substituting this expression into the Eq. (21), we have

$$\sigma^a = \int d^2\mathbf{b} e^{-\sigma_0 D_A(\mathbf{b})} \sum_{n=1}^{\infty} \frac{1}{n!} \prod_{i=1}^n \left[\int d\varepsilon_{Ti} \frac{d\sigma_0}{d\varepsilon_{Ti}} D_A(\mathbf{b}) \right], \quad (23)$$

and thus the total transverse energy distribution is

$$\begin{aligned} \frac{d\sigma}{dE_T} &= \int d^2\mathbf{b} e^{-\sigma_0 D_A(\mathbf{b})} \sum_{n=1}^{\infty} \frac{1}{n!} \prod_{i=1}^n \\ &\times \left[\int d\varepsilon_{Ti} \frac{d\sigma_0}{d\varepsilon_{Ti}} D_A(\mathbf{b}) \right] \delta(E_T - \varepsilon_{T1} - \dots - \varepsilon_{Tn}). \end{aligned} \quad (24)$$

Using

$$\delta(E_T - \varepsilon_{T1} - \dots - \varepsilon_{Tn}) = \frac{1}{2\pi} \int d\tau e^{i(E_T - \varepsilon_{T1} - \dots - \varepsilon_{Tn})\tau}, \quad (25)$$

it gives

$$\begin{aligned} \frac{d\sigma}{dE_T} &= \int d^2\mathbf{b} \frac{1}{2\pi} \int d\tau e^{iE_T\tau} \left[\exp\left(D_A(\mathbf{b}) \right. \right. \\ &\times \left. \left. \int d\varepsilon_T \frac{d\sigma_0}{d\varepsilon_T} (e^{-i\varepsilon_T\tau} - 1) \right) - 1 \right]. \end{aligned} \quad (26)$$

Because the transverse energy ε_T created in each particle-particle collision is small, even the total transverse energy E_T is large, we have, approximately,

$$e^{-i\varepsilon_T\tau} \approx 1 - i\varepsilon_T\tau - \frac{1}{2}\varepsilon_T^2\tau^2, \quad (27)$$

and obtain for $E_T \neq 0$ finally

$$\frac{d\sigma}{dE_T} \approx \int dE_T^g \frac{d^2\mathbf{b}}{dE_T^g} \frac{1}{\sqrt{2\pi\Delta(\mathbf{b})}} e^{-[E_T - E_T^g(\mathbf{b})]^2/2\Delta^2(\mathbf{b})}. \quad (28)$$

In the above formula,

$$E_T^g = E_T^g(\mathbf{b}) = \int d\varepsilon_T \varepsilon_T \frac{d\sigma_0}{d\varepsilon_T} D_A(\mathbf{b}) = \bar{\varepsilon}_T \sigma_0 D_A(\mathbf{b}) \quad (29)$$

TABLE I. The model parameters σ_0 (in mb), $\bar{\varepsilon}_T$ (in GeV), and $\overline{\varepsilon_T^2}$ (in GeV^2) fitted to the measured data, and the calculated geometric energy E_T^g and E_F^g at head-on and dive-in points, in GeV. The data of 158A GeV $^{208}\text{Pb}+\text{Pb}$ are taken from the NA49 Collaboration [32]; the data of the other systems are taken from the NA35 Collaboration [29]. The results under ‘‘Other,’’ taken from Refs. [32] and [29], are from the NA49 Collaboration for 158A GeV $^{208}\text{Pb}+\text{Pb}$ and FRITIOF for other systems.

	System	σ_0	$\bar{\varepsilon}_T$	$\overline{\varepsilon_T^2}$	$E_T^g(0)$			$E_F^g(0)$		$E_T^g(b_{DI})$		$E_F^g(b_{DI})$
					Data	Present	Other	Present	Data	Present	Other	Present
60A GeV	$^{16}\text{O}+\text{Au}$	33.83	0.531	0.704	54.8	54.1	54.5	2.6	42.8	40.4	44.3	45.4
	Ag	38.44	0.566	0.611	51.2	50.5	50.2	8.3	42.4	41.0	42.5	50.7
	Cu	28.70	0.888	0.870	46.8	45.4	44.9	58.8	41.7	39.9	40.5	108.5
158A GeV	$^{208}\text{Pb}+\text{Pb}$	13.76	1.295	1.781		527.1	520	6450.3		527.1	520	6450.3
200A GeV	$^{16}\text{O}+\text{Au}$	18.57	1.594	2.190	88.6	89.1	88.5	105.2	66.7	66.6	68.4	388.3
200A GeV	$^{32}\text{S}+\text{Au}$	14.20	2.066	3.031	170	171.3	160	512.3	145	142.0	136	992.7
	Ag	14.37	2.232	4.274	145	140.9	140	986.2	131	126.6	127	1326.3
	Cu	16.48	2.183	3.264	121	117.5	117	1394.4	121	112.8	117	1538.7
	S	18.06	2.194	4.441	87	81.5	82.5	2356.1		81.5		2356.1

is the geometric transverse energy created in the $p+A$ collision at the impact parameter \mathbf{b} , and $\Delta(\mathbf{b})$ is the width of the Gaussian distribution of the measured transverse energy E_T around the value $E_T^g(\mathbf{b})$,

$$\Delta^2(\mathbf{b}) = \int d\varepsilon_T \varepsilon_T^2 \frac{d\sigma_0}{d\varepsilon_T} D_A(\mathbf{b}) = \overline{\varepsilon_T^2} \sigma_0 D_A(\mathbf{b}), \quad (30)$$

where $\bar{\varepsilon}_T$ and $\overline{\varepsilon_T^2}$ are the first and the second moments of the transverse energy ε_T over its distribution $d\sigma_0/d\varepsilon_T$, respectively,

$$\bar{\varepsilon}_T = \frac{1}{\sigma_0} \int d\varepsilon_T \varepsilon_T \frac{d\sigma_0}{d\varepsilon_T}, \quad \overline{\varepsilon_T^2} = \frac{1}{\sigma_0} \int d\varepsilon_T \varepsilon_T^2 \frac{d\sigma_0}{d\varepsilon_T}. \quad (31)$$

Formula (28) says that the total transverse energy distribution $d\sigma/dE_T$ of the collision $p+A$ can be expressed by its geometric distribution $d^2\mathbf{b}/dE_T^g$ convoluted by a Gaussian distribution with centroid E_T^g and width $\Delta(\mathbf{b})$. In this case, the geometric distribution is a result of the collision kinematics and dynamics, while the Gaussian distribution is mainly due to the statistical behavior of the quantum many-body collisions involved.

For the high energy nucleus-nucleus collision $B+A$, the following assumptions can be invoked as the bases of our model: (1) The projectile B and the target A are built up by the same type of particles, (2) each projectile particle is scattered by the target in the way described above, and (3) the total collision $B+A$ is the incoherent summation of these projectile particle collisions with the target. In this way, the transmission coefficient $S_{pA}(\mathbf{b})$ is changed to $S_{BA}(\mathbf{b})$,

$$S_{BA}(\mathbf{b}) = e^{-\sigma_0 D_{BA}(\mathbf{b})}, \quad (32)$$

and thus the formula (28) can be extended to the $B+A$ collision by changing $D_A(\mathbf{b})$ to the thickness distribution function $D_{BA}(\mathbf{b})$ of the collision $B+A$,

$$D_{BA}(\mathbf{b}) = \int d^2\mathbf{s} D_B(\mathbf{s}) D_A(\mathbf{b}+\mathbf{s}), \quad (33)$$

where $D_B(\mathbf{s})$ is the thickness distribution function of the nucleus B with density $\rho_B(\mathbf{r})$ normalized to B ,

$$D_B(\mathbf{s}) = \int \rho_B(\mathbf{s}, z) dz, \quad B = \int d^3\mathbf{r} \rho_B(\mathbf{r}). \quad (34)$$

The formula (28) extended to the collision $B+A$ will be referred to hereafter as the extended equation (28). It provides a physical argument for the earlier analysis [27] which suggested that, for the heaviest targets, the plateau of the transverse energy distribution ends in a bump which is followed by a rapidly falling tail of Gaussian shape. Furthermore, the present result shows that this tail is basically the statistical behavior of quantum many-body collisions. It is interesting to note that this formula is the same as that used in Ref. [28] and similar to that used in Refs. [17] and [18] for data fitting.

IV. FORWARD ENERGY DISTRIBUTION

Because of the attenuation of the transmission coefficient $S_{pA}(\mathbf{b})$, the geometric forward energy of the collision $p+A$ at the impact parameter \mathbf{b} can be written as

$$E_F^g = E_F^g(\mathbf{b}) = E_n e^{-\sigma_0 D_A(\mathbf{b})}, \quad (35)$$

where the projectile p is considered as a point particle, and E_n is its kinetic energy. For the nucleus-nucleus collision $B+A$, by the incoherence assumption, the expression of the geometric forward energy can be written as

$$E_F^g = E_F^g(\mathbf{b}) = \int d^2\mathbf{s} D_B(\mathbf{s}) E_n e^{-\sigma_0 D_A(\mathbf{b}+\mathbf{s})}. \quad (36)$$

A correlation between the transverse energy E_T and the forward energy E_F is observed experimentally [29]. Assuming a one-to-one correspondence $E_T \sim E_F$, the following relation between the forward and the transverse energy distributions can be written:

$$\frac{d\sigma}{dE_F} = \frac{dE_T}{dE_F} \frac{d\sigma}{dE_T}. \quad (37)$$

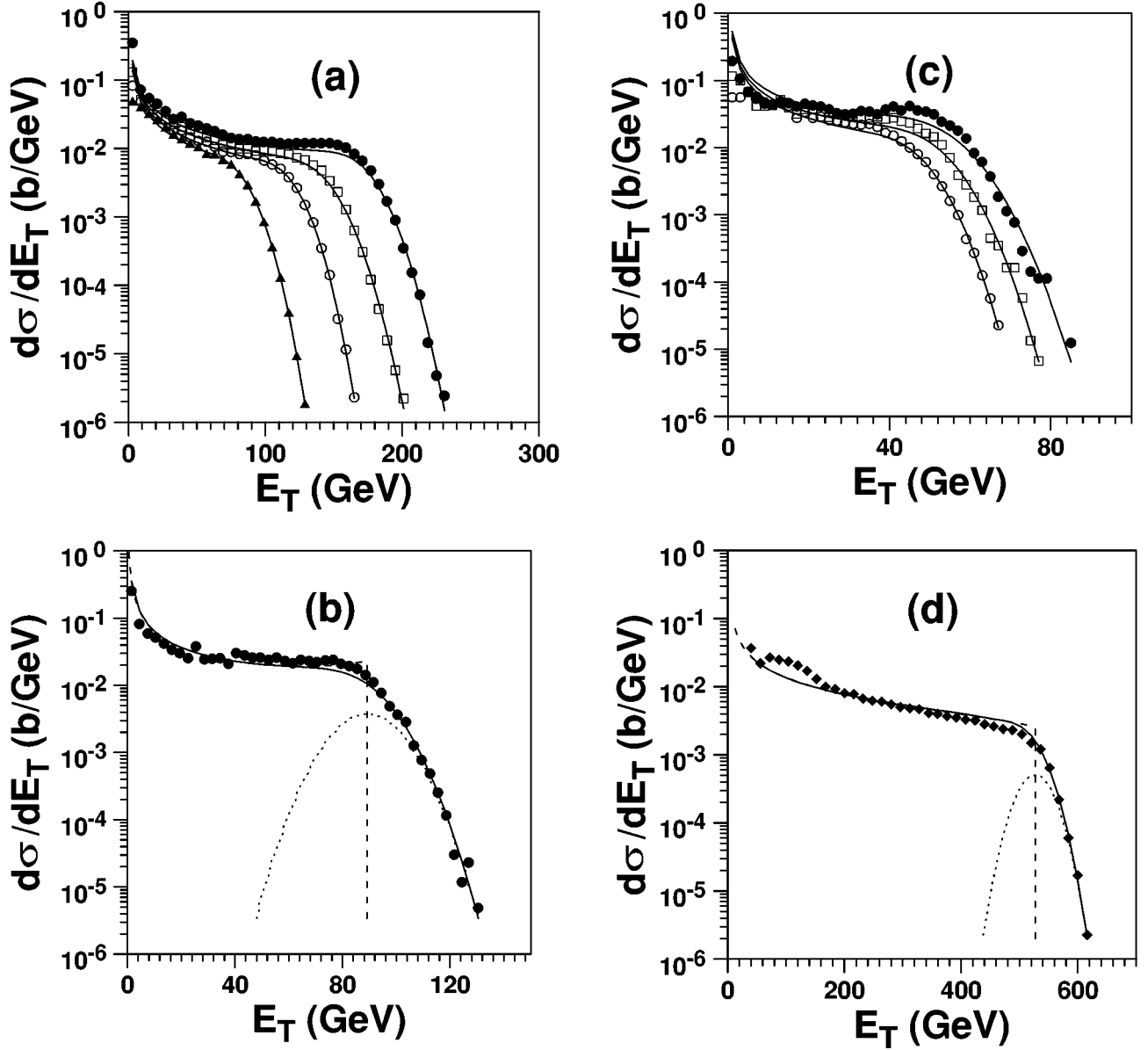


FIG. 1. The transverse energy distributions $d\sigma/dE_T$ for (a) $^{32}\text{S}+\text{Au}$, Ag, Cu, and S at 200A GeV, (b) $^{16}\text{O}+\text{Au}$ at 200A GeV, (c) $^{16}\text{O}+\text{Au}$, Ag, and Cu at 60A GeV, and (d) $^{208}\text{Pb}+\text{Pb}$ at 158A GeV. The measured data are taken from the NA49 Collaboration [31,32] for Pb+Pb (the solid diamonds) and NA35 Collaboration [29] for others (the solid dots stand for Au, the open squares for Ag, the circles for Cu, and the triangles for S targets). The solid curves are calculated by the extended equation (28). In (b) and (d), the dashed curves are the corresponding geometric distributions, and the dotted curves are the convoluted Gaussian distributions centered at the end of the geometric distribution $E_T^g(0)$ with the corresponding widths, i.e., $\Delta(0)=11.06$ GeV for (b) and $\Delta(0)=26.93$ GeV for (d), as well as with the appropriate normalization. The fitted parameters are given in Table I.

Substituting the extended equation (28) into the above equation, and making the approximation $(E_T - E_T^g) \approx (E_F - E_F^g)/\eta$, where $\eta = (dE_F/dE_T)_g$ and g stands for $E_T = E_T^g$ as well as $E_F = E_F^g$, the following formula can be obtained:

$$\frac{d\sigma}{dE_F} \approx \int dE_F^g \frac{d^2\mathbf{b}}{dE_F^g} \frac{1}{\sqrt{2\pi}\Delta_F(\mathbf{b})} e^{-[E_F - E_F^g(\mathbf{b})]^2/2\Delta_F^2(\mathbf{b})}, \quad (38)$$

where

$$\Delta_F(\mathbf{b}) = \eta\Delta(\mathbf{b}). \quad (39)$$

Similar to the extended equation (28), the formula (38) says that the total forward energy distribution $d\sigma/dE_F$ of the collision $B+A$ can be expressed by its geometric distribution $d^2\mathbf{b}/dE_F^g$ convoluted by a Gaussian distribution with centroid E_F^g and width $\Delta_F(\mathbf{b})$. The information of the collision kinematics and dynamics is also involved mainly in the geometric distribution, while the statistical behavior of quantum many-body collision processes is involved in the Gaussian

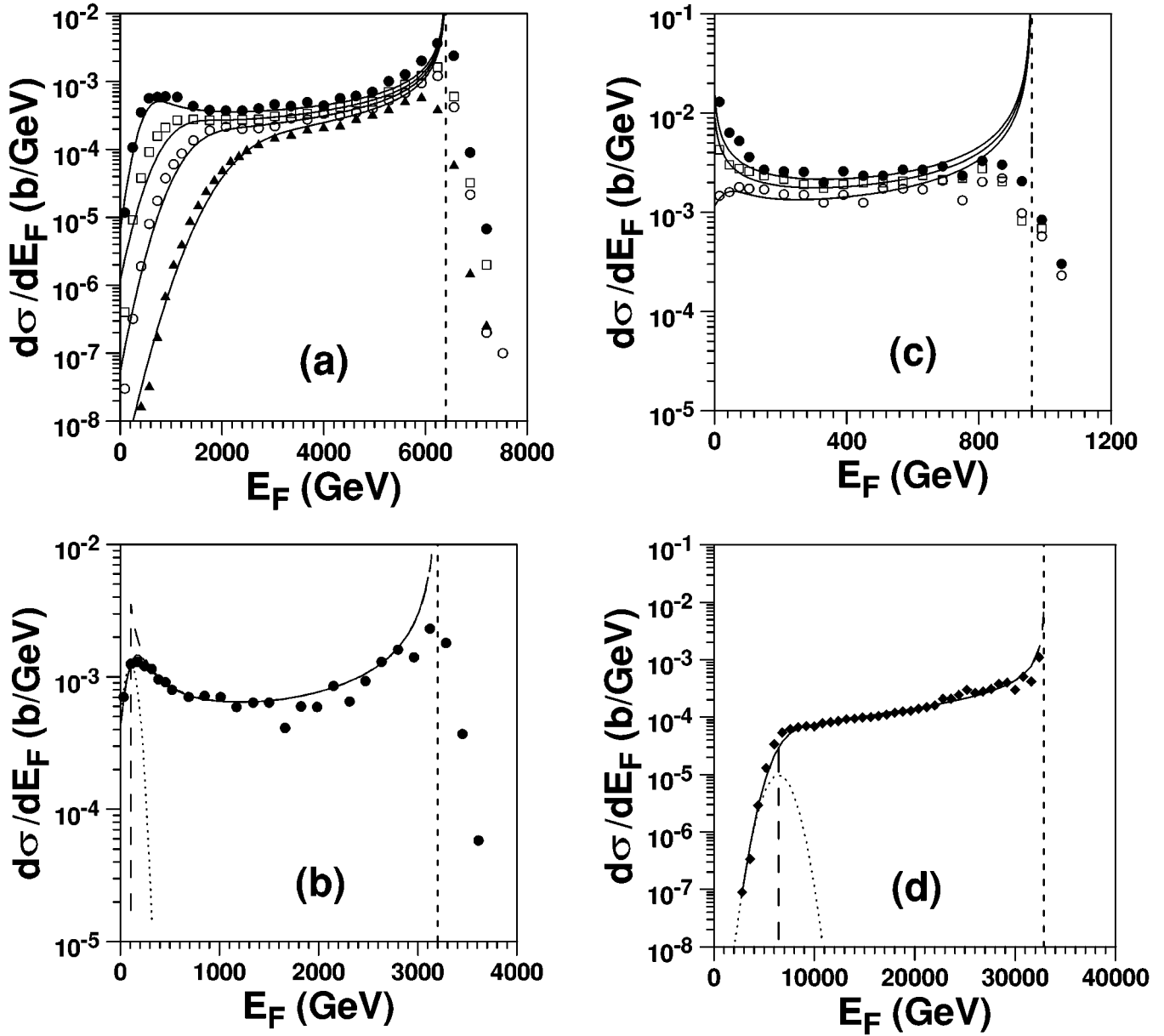


FIG. 2. The forward energy distributions $d\sigma/dE_F$ for (a) $^{32}\text{S}+\text{Au}$, Ag, Cu, and S at 200A GeV, (b) $^{16}\text{O}+\text{Au}$ at 200A GeV, (c) $^{16}\text{O}+\text{Au}$, Ag, and Cu at 60A GeV, and (d) $^{208}\text{Pb}+\text{Pb}$ at 158A GeV. The measured data are taken from the NA49 Collaboration [31,32] for Pb+Pb (the solid diamonds) and NA35 Collaboration [29] for others (the solid dots stand for Au, the open squares for Ag, the circles for Cu, and the triangles for S targets). The solid curves are calculated by Eq. (38). The vertical short dashed lines correspond to the beam energies BE_n . In (b) and (d), the long dashed curves are the corresponding geometric distributions, and the dotted curves are the convoluted Gaussian distributions centered at the end of the geometric distribution $E_F^g(0)$ with the corresponding widths, i.e. $\Delta_F(0)=71.41$ GeV for (b) and $\Delta_F(0)=1189.41$ GeV for (d), as well as with the appropriate normalization. The fitted parameters are given in Table I.

distribution. In a practical application, such as will be shown in the next section, the factor η can be approximated as

$$\eta = \left(\frac{dE_F}{dE_T} \right)_g \approx \frac{dE_F^g}{dE_T^g}. \quad (40)$$

It is interesting to note that the formula of the forward energy distribution given in Ref. [10] is essentially the geometric distribution similar to our $d^2\mathbf{b}/dE_F^g$ which appears in the formula (38).

V. NUMERICAL EXAMPLES

The projectile and target nucleon numbers are chosen as B and A , respectively, in the present calculation. In this case σ_0 is a parameter which is related to the N - N collision. The nuclear density $\rho_{B,A}(r)$ is assumed to be the Fermi distribution, where the central radius and surface diffuseness are calculated with the nuclear radius constant $r_0=1.16$ fm and the Süssmann width $b=1.0$ fm [30].

The relevant quantities appeared in the formulas (28) and (38) are $\bar{\varepsilon}_T$, ε_T^2 , σ_0 , $D_{BA}(\mathbf{b})$, and η . In a practical application, $\bar{\varepsilon}_T$, ε_T^2 , and σ_0 can be used as adjustable parameters

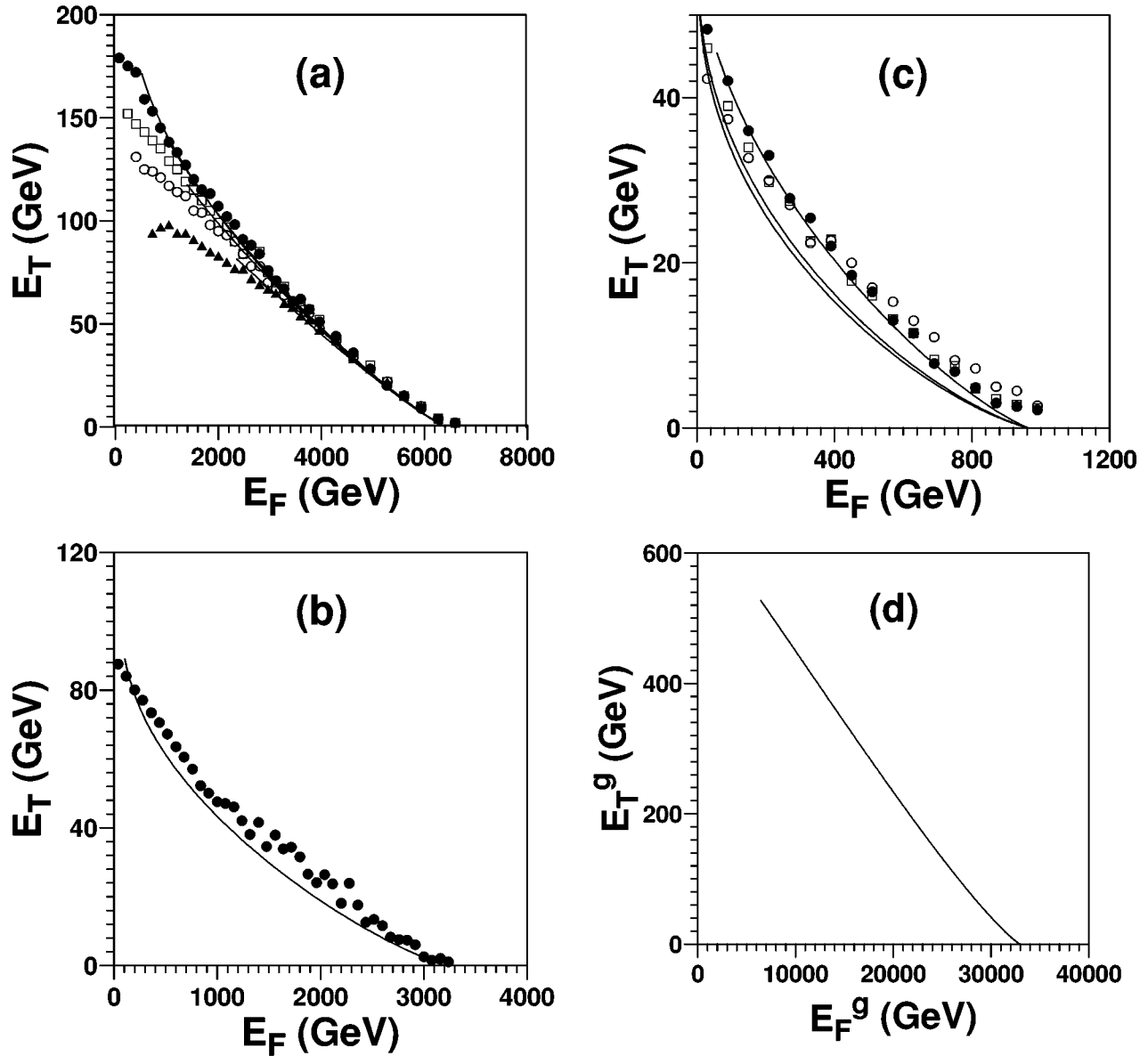


FIG. 3. The correlations $E_T \sim E_F$ for (a) $^{32}\text{S}+\text{Au}$, Ag, Cu, and S at 200A GeV, (b) $^{16}\text{O}+\text{Au}$ at 200A GeV, (c) $^{16}\text{O}+\text{Au}$, Ag, and Cu at 60A GeV, and (d) $^{208}\text{Pb}+\text{Pb}$ at 158A GeV. The measured data are taken from the NA35 Collaboration [29] (the solid dots stand for Au, the open squares for Ag, the circles for Cu, and the triangles for S targets). The measured data for Pb+Pb given by the NA49 Collaboration [31] are not plotted here. The solid curves are calculated by Eqs. (29) and (36). The parameters used are fitted to the transverse and forward energy distributions. The measured error bars, which are about ± 5 to ± 10 GeV, are not plotted here.

fitted to the measured distributions, and D_{BA} (b) and η can be calculated if the nuclear density $\rho_{B,A}(\mathbf{r})$ is known. In the calculation shown in this section, $\sigma_0 \bar{\varepsilon}_T$ and $\sigma_0 \varepsilon_T^2$ are determined by the measured transverse energy distribution at first, and then σ_0 by the measured forward energy distribution, in a least-squares fitting. In this determination, $\sigma_0 \bar{\varepsilon}_T$ is determined mainly by the end of the plateau of the transverse energy distribution, and $\sigma_0 \varepsilon_T^2$ mainly by the width of the distribution tail, while σ_0 is determined mainly by the initial of the plateau of the forward energy distribution. The fitted parameters are given in Table I.

Figure 1 shows the transverse energy distributions $d\sigma/dE_T$ for (a) $^{32}\text{S}+\text{Au}$, Ag, Cu, and S at 200A GeV, (b) $^{16}\text{O}+\text{Au}$ at 200A GeV, (c) $^{16}\text{O}+\text{Au}$, Ag, and Cu at 60A GeV, and (d) $^{208}\text{Pb}+\text{Pb}$ at 158A GeV. The measured data

are taken from the NA49 Collaboration [31,32] for Pb+Pb (the solid diamonds) and NA35 Collaboration [29] for others (the solid dots stand for Au, the open squares for Ag, the circles for Cu, and the triangles for S targets). The solid curves are calculated by the extended equation (28). In (b) and (d), the dashed curves are the corresponding geometric distributions, and the dotted curves are the convoluted Gaussian distributions centered at the end of the geometric distribution $E_T^g(0)$ with the corresponding widths, i.e., $\Delta(0) = 11.06$ GeV for (b) and $\Delta(0) = 26.93$ GeV for (d), as well as with the appropriate normalization.

Figure 2 shows the forward energy distributions $d\sigma/dE_F$ for (a) $^{32}\text{S}+\text{Au}$, Ag, Cu, and S at 200A GeV, (b) $^{16}\text{O}+\text{Au}$ at 200A GeV, (c) $^{16}\text{O}+\text{Au}$, Ag, and Cu at 60A GeV, and (d) $^{208}\text{Pb}+\text{Pb}$ at 158A GeV. The measured data are taken from the NA49 Collaboration [31,32] for Pb+Pb (the solid dia-

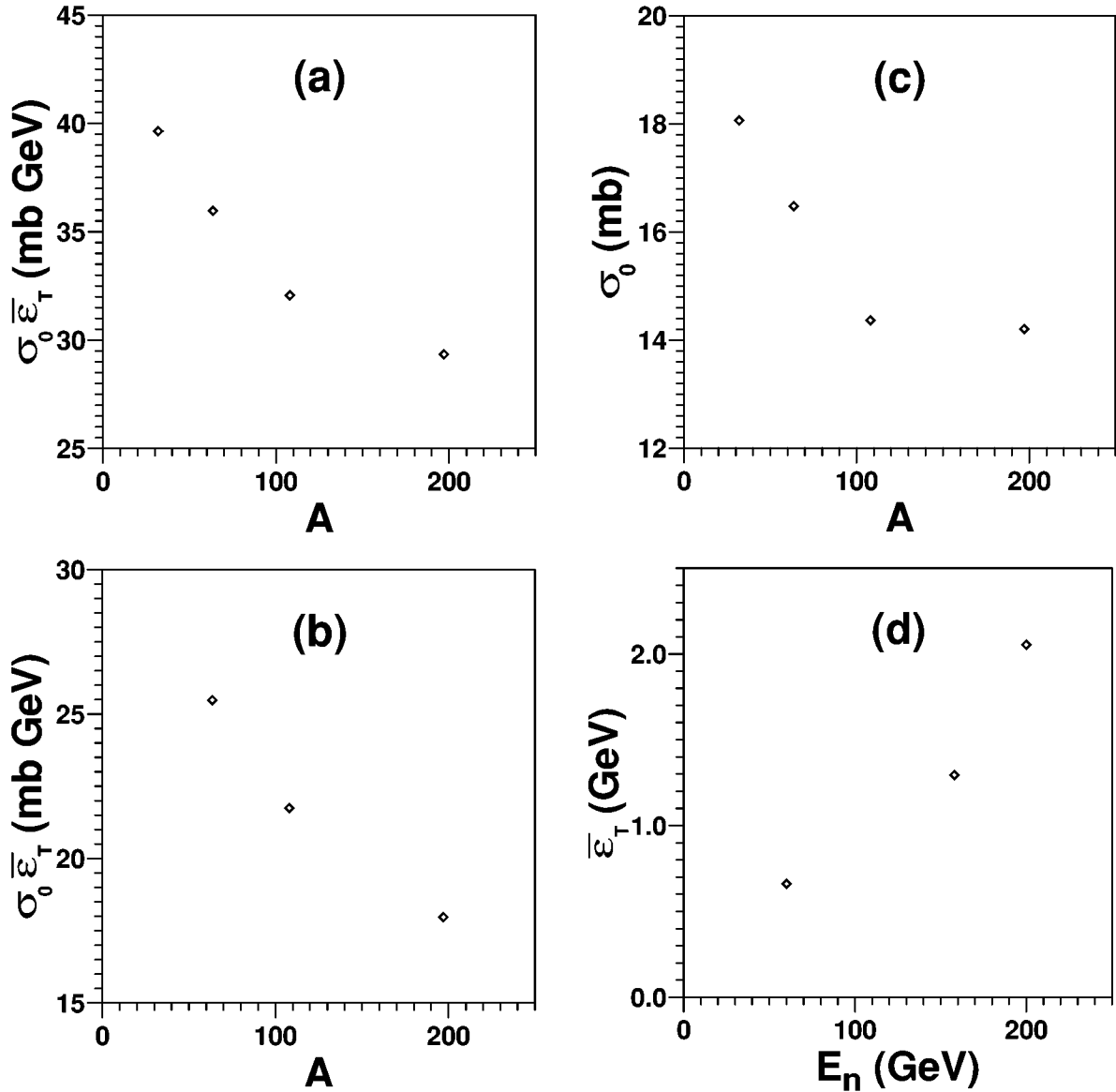


FIG. 4. The systematics of the fitted parameters: (a) $\sigma_0 \bar{\epsilon}_T$ versus A for $^{32}\text{S}+A$ at 200A GeV, (b) $\sigma_0 \bar{\epsilon}_T$ versus A for $^{16}\text{O}+A$ at 60A GeV, (c) σ_0 versus A for $^{32}\text{S}+A$ at 200A GeV, and (d) the averaged $\bar{\epsilon}_T$ versus the nucleon projectile energy E_n .

monds) and NA35 Collaboration [29] for others (the solid dots stand for Au, the open squares for Ag, the circles for Cu, and the triangles for S targets). The solid curves are calculated by Eq. (38). The vertical short dashed lines correspond to the beam energies BE_n . In (b) and (d), the long dashed curves are the corresponding geometric distributions, and the dotted curves are the convoluted Gaussian distributions centered at the end of the geometric distribution $E_F^g(0)$ with the corresponding widths, i.e., $\Delta_F(0)=71.41$ GeV for (b) and $\Delta_F(0)=1189.41$ GeV for (d), as well as with the appropriate normalization.

The correlations $E_T \sim E_F$ are shown in Fig. 3 for (a) $^{32}\text{S}+\text{Au}$, Ag, Cu, and S at 200A GeV, (b) $^{16}\text{O}+\text{Au}$ at 200A GeV, (c) $^{16}\text{O}+\text{Au}$, Ag, and Cu at 60A GeV, and (d) $^{208}\text{Pb}+\text{Pb}$ at 158A GeV. The measured data are taken from the NA35 Collaboration [29] (the solid dots stand for Au, the open squares for Ag, the circles for Cu, and the triangles for S targets). The measured data for Pb+Pb given by the NA49 Collaboration [31] are not plotted here. The solid curves are

calculated by Eqs. (29) and (36). The parameters used in this calculation are the above-mentioned ones fitted to the transverse and forward energy distributions. It should be emphasized that the calculated curves are for the geometric quantities E_T^g and E_F^g but not for the measured ones E_T and E_F . Especially, there is a lower limit for the geometric forward energy which is higher than the lowest measured forward energy, as can be seen from Fig. 3(a). However, the agreement between the calculation and the measurement is satisfactory within the measured error bars, which are about ± 5 to ± 10 GeV and not plotted here, and thus supports the applicability of approximation (40).

As the measurement outputs are calorimeter dependent, the fitted parameters are expected to be also calorimeter-dependent constants [17,18]. As a consequence, the fitted σ_0 cannot be understood as the effective total $N-N$ cross section in its exact meaning. However, it is interesting to investigate the systematics of the parameters σ_0 , $\bar{\epsilon}_T$, and $\bar{\epsilon}_T^2$, even in the present case with only a few points. It can be seen from

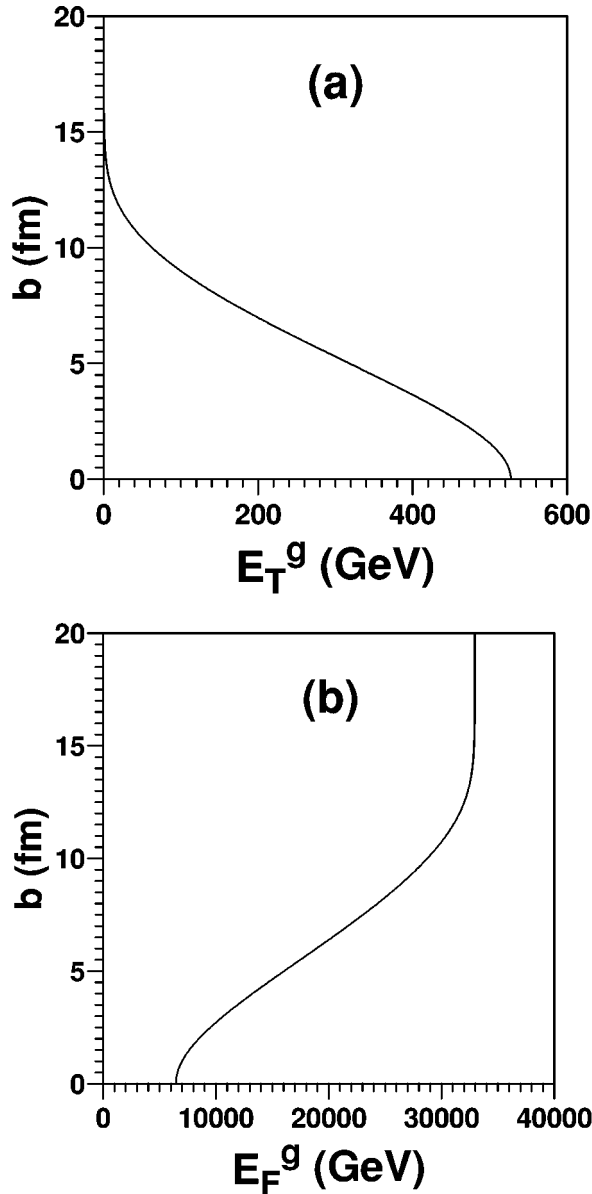


FIG. 5. The correlations of the impact parameter b versus (a) the geometric transverse energy E_T^g and (b) the geometric forward energy E_F^g of a 158A GeV $^{208}\text{Pb}+\text{Pb}$ collision.

Table I that the parameters $\bar{\varepsilon}_T$ and $\overline{\varepsilon_T^2}$ increase with the projectile nucleon energy E_n obviously, but are independent of the target number of nucleons A for a given projectile B approximately. The large scattering of ε_T^2 values in this case may be understood by the deformation of the target nuclei, which has more influence on ε_T^2 than on $\bar{\varepsilon}_T$ and is not considered in the present calculation. On the other hand, σ_0 seems to decrease with the target A for a given projectile B approximately. In this regard, it should be kept in mind that σ_0 is determined mainly by the initial of the plateau of the forward energy distribution. In the case of $^{16}\text{O}+\text{Au}$, Ag , and Cu at 60A GeV, this determination is not so reliable due to the lack of measured points in the initial region. However, the decreasing of σ_0 is obvious from the fitted $\sigma_0\bar{\varepsilon}_T$ if $\bar{\varepsilon}_T$ is assumed to be constant independent of the target A . Figure 4 plots the systematics of the fitted parameters: (a) $\sigma_0\bar{\varepsilon}_T$ versus

A for $^{32}\text{S}+\text{A}$ at 200A GeV, (b) $\sigma_0\bar{\varepsilon}_T$ versus A for $^{16}\text{O}+\text{A}$ at 60A GeV, (c) σ_0 versus A for $^{32}\text{S}+\text{A}$ at 200A GeV, and (d) the averaged $\bar{\varepsilon}_T$ versus the nucleon projectile energy E_n . The plots of $\sigma_0\overline{\varepsilon_T^2}$, considering the large scattering of ε_T^2 mentioned above, are similar to that of $\sigma_0\bar{\varepsilon}_T$ and not shown here.

The significant difference of $\bar{\varepsilon}_T$ between $^{32}\text{S}+\text{Au}$ and $^{16}\text{O}+\text{Au}$ at 200A GeV, as shown in Table I, may be understood in a similar way. We keep this as an open problem for further study. In this consideration, the fitting to more measured data, for example, the data of the WA80 Collaboration [33], will be helpful.

Figure 5 shows the correlations of the impact parameter b versus the geometric transverse energy E_T^g (a) and geometric forward energy E_F^g (b) of a 158A GeV $^{208}\text{Pb}+\text{Pb}$ collision, respectively. As the measured transverse and forward energy E_T and E_F are spread out around the geometric ones E_T^g and E_F^g , respectively, in a Gaussian distribution with the width proportional to the collision thickness function $D_{BA}(\mathbf{b})$, the correlation of the impact parameter b versus the measured transverse energy E_T and forward energy E_F is ambiguous since it is not a simple single-valued function. Therefore, the use of global observables, at least the transverse and the forward energy, as the centrality cut in the experimental measurements must be taken carefully, especially in the central collision $b \approx 0$ case.

Besides the head-on collision point $b=0$, a dive-in point is defined at $b_{\text{DI}}=R_{\text{target}}-R_{\text{projectile}}$ in the literature [29]. Table I gives the calculated geometric energy at these two points, in comparison with the data of NA35 Collaboration [29] and the FRITIOF calculation [29].

VI. DISCUSSION AND SUMMARY

As a phenomenological approach to the transverse and the forward energy distributions, the present formalism is general enough, since it is independent of what is assumed as elemental constituent particles. As a matter of fact, instead of nucleons a similar calculation by using the parton picture may be performed. A result without essential changes can be expected. The present work shows that global observables, at least the transverse and the forward energy distributions, are related to only a few global degrees of freedom of the colliding system. In other words, only a few global properties of the colliding system, i.e., the collision geometry and kinematics as well as the average properties of the collision dynamics, can be learned from these global observables, while the details of the collision process are nonrelevant for these global observables. In this respect, the systematics of the model parameters $\bar{\varepsilon}_T$ and $\overline{\varepsilon_T^2}$ will provide some information about the collision dynamics.

It can be seen from Eq. (33) that the thickness distribution function $D_{BA}(\mathbf{b})$ is proportional to the total number of binary collisions, and so the main ingredient in our formulas (28) and (38) is the number of binary collisions, similar to the models used in some data fittings [28,34]. However, as σ_0 is shown to decrease with the target A , and probably also with the projectile B , it seems that one of our basic assumptions (14) should be modified to include also the second term for

the surface effect of the collision. In this way, the expression of $D_{BA}(\mathbf{b})$ will be modified correspondingly. Physically, this corresponds to substituting the number of binary collisions with another kind of number, which may be similar to the number of wounded projectile nucleons [5,35–37]. Furthermore, if $\bar{\epsilon}_T$ is proved to be correlated to the projectile B , our other basic assumption, i.e., the incoherence assumption, should be modified also. We will address these points quantitatively in the next step of our study.

In conclusion, the main results of the present work can be summarized as follows.

(1) The transverse and the forward energy distributions can be expressed, respectively, by their geometric distribution convoluted by a Gaussian distribution with centroid and width determined by the collision geometry and the average properties of N - N collisions. In other words, the transverse and the forward energy distributions can be expressed, respectively, essentially by their geometric distribution, except the head-on collision tail which is basically a Gaussian distribution.

(2) The plateau of the transverse energy distribution,

which is essentially the geometric distribution, is proportional to the collision thickness function $D_{BA}(\mathbf{b})$.

(3) The widths of the head-on collision tail of the transverse and the forward energy distributions are proportional to the square root of the collision thickness function $D_{BA}(\mathbf{b})$.

(4) The measured transverse energy E_T and forward energy E_F correspond to a variety of impact parameters b , which spread on a Gaussian distribution with the width proportional to the square root of the collision thickness function $D_{BA}(\mathbf{b})$. Therefore, the centrality cut of the collision should be considered carefully in connection with a model-dependent calculation.

ACKNOWLEDGMENTS

One of us (C.S.W.) is supported partly by the National Natural Science Foundation of China and the Special Fund of China for the Universities with Ph.D. Programs. He would like to acknowledge support from the Fundação de Amparo à Pesquisa do Estado do Rio de Janeiro (FAPERJ).

-
- [1] *Proceedings of Quark Matter '96*, edited by P. Braun-Munzinger, H.J. Specht, R. Stock, and H. Stöcker [Nucl. Phys. **A610** (1996)].
- [2] NA50 Collaboration, Michel Gonin *et al.*, Nucl. Phys. **A610**, 404c (1996).
- [3] Carlos Lourenço, Nucl. Phys. **A610**, 552c (1996).
- [4] C.Y. Wong, in *Proceedings of the Tenth INS-Kikuchi Spring School on Quarks and Nuclei*, edited by O. Hashimoto and F. Sakata, Shimoda, Japan, 1987 (unpublished).
- [5] J. Ftáčnik, K. Kajantie, N. Pišťová, and J. Pišť, Phys. Lett. B **188**, 279 (1987).
- [6] Gordon Baym, Peter Braun-Munzinger, and Vesa Ruuskanen, Phys. Lett. B **190**, 29 (1987).
- [7] A.D. Jackson and H. Bøggild, Nucl. Phys. **A470**, 669 (1987).
- [8] M. Kutschera, J. Hüfner, and K. Werner, Phys. Lett. B **192**, 283 (1987).
- [9] K. Werner, Z. Phys. C **38**, 193 (1988).
- [10] S.K. Gupta, Z. Phys. A **331**, 457 (1988).
- [11] S.K. Gupta, Phys. Rev. C **39**, 737 (1989).
- [12] A.J. Baltz, Phys. Rev. C **43**, 1420 (1991); Nucl. Phys. **A525**, 639c (1991).
- [13] R. Shanta and S.K. Gupta, Z. Phys. A **338**, 183 (1991).
- [14] Den-Zhi Zhang and Cheng-Shing Wang, Phys. Rev. C **45**, 1356 (1992).
- [15] Cheng-Shing Wang and Kan-Zhu Guo, Phys. Rev. C **48**, 379 (1993).
- [16] B. Shiva-Kumar, S.V. Greene, and J.T. Mitchell, Phys. Rev. C **50**, 2152 (1994).
- [17] D. Kharzeev, Nucl. Phys. **A610**, 418c (1996).
- [18] Sean Gavin and Ramona Vogt, Nucl. Phys. **A610**, 442c (1996).
- [19] Charles J. Joachin, *Quantum Collision Theory* (North-Holland, Amsterdam, 1975).
- [20] R.J. Glauber, in *Lectures in Theoretical Physics*, edited by W.E. Brittin *et al.* (Interscience, New York, 1959), Vol. I, p. 315.
- [21] R.J. Glauber, in *High-Energy Physics and Nuclear Structure, Proceedings of the 2nd International Conference*, Rehovoth, 1967, edited by G. Alexander (North-Holland, Amsterdam, 1967), p. 311.
- [22] C.Y. Wong, Phys. Rev. D **30**, 972 (1984).
- [23] V.N. Gribov, Sov. Phys. JETP **30**, 709 (1970).
- [24] L. Bertocchi, Nuovo Cimento A **11**, 45 (1972).
- [25] A.M. Perey and F.G. Perey, At. Data Nucl. Data Tables **17**, 1 (1976).
- [26] T.T. Chou and C.N. Yang, Phys. Rev. **170**, 1591 (1968).
- [27] WA80 Collaboration, R. Albrecht *et al.*, Z. Phys. C **45**, 31 (1989).
- [28] T. Åkesson *et al.*, Z. Phys. C **38**, 383 (1988).
- [29] NA35 Collaboration, J. Bächler *et al.*, Z. Phys. C **52**, 239 (1991).
- [30] R.W. Hasse and W.D. Myers, *Geometrical Relationships of Macroscopic Nuclear Physics* (Springer-Verlag, New York, 1988).
- [31] S. Margetis *et al.*, Nucl. Phys. **A590**, 355c (1995).
- [32] T. Alber *et al.*, Phys. Rev. Lett. **75**, 3814 (1995).
- [33] R. Albrecht *et al.*, Phys. Rev. C **44**, 2736 (1991).
- [34] K.J. Eskola, K. Kajantie, and J. Lindfors, Nucl. Phys. **B323**, 37 (1989).
- [35] A. Bamberger *et al.*, Phys. Lett. B **184**, 271 (1987).
- [36] T. Abbott *et al.*, Phys. Lett. B **197**, 285 (1987).
- [37] T. Abbott *et al.*, Phys. Rev. C **45**, 2933 (1992).